Effects of Redshift on the Classifying Criteria of BL Lacertae Objects[*]

Li Ma[1,3], Luo-En Chen[2,3], Guang-Zhong Xie[3,4], Ji-Yang Ren[2], Zhao-Hua Xie[1],
Shu-Bai Zhou[3,4], Hui Wu[1] and Dong-Cheng Mei[4]

[1] Department of Physics, Yunnan Normal University, Kunming 650092; *astromali@126.com*
[2] Department of Physics, Yuxi Normal College, Yuxi 653100
[3] National Astronomical Observatories/ Yunnan Observatory, Chinese Academy of Sciences, Kunming 650011
[4] Department of Physics, Yunnan University, Kunming 650091

Abstract We have collected a sample of 70 BL Lacs (33 radio-selected BL Lacs and 37 X-ray selected BL Lacs) with multi-waveband data for investigating the classifying criteria of BL Lacertae Objects. For each source, we estimate its luminosities in radio, optical and X-ray, the broad-band spectral index from radio to X-ray and the peak frequency of the synchrotron emission, and make a statistical analysis of the data obtained. Our main results are as follows: (1) The broad-band spectral index and the peak frequency have no correlation with the redshift, while they are inversely correlated with each other and they could be regarded as equivalent classifying criteria of BL Lac objects. (2) There are significant effects of the luminosity/redshift relation on the observed luminosity distribution in our sample, hence, if the radio luminosity is to be used as a classifying criterion of BL Lac objects, it should not be regarded as equivalent to the broad-band spectral index or the peak frequency. (3) Our results supply a specific piece of evidence for the suggestion that the use of luminosities always introduces a redshift bias to the data and show that the location of the peak frequency is not always linked to the luminosity of any wave band.

Key words: galaxies: BL Lacertae objects: general—galaxies: fundamental parameters—galaxies: high-redshift

1 INTRODUCTION

Radio-selected BL Lac objects (RBLs) and X-ray-selected BL Lac objects (XBLs) are two subclasses of BL Lacertae objects, that are respectively observed and identified by radio and X-ray surveys. There are many significant differences between these two subclasses (Ledden & O'Dell 1985; Ghisellini et al. 1986; Stocke et al. 1991; Xie et al. 2001a, 2003), and some of them are difficult to be accounted for by the observational threshold only (Qin & Xie 1997). The classifying criteria of these subclasses have been widely studied based on the differences. For example, the difference in their spectral energy distributions shows that RBL-like sources occupy the region of $\alpha_{\mathrm{rx}} > 0.75$, and XBL-like sources, the region of $\alpha_{\mathrm{rx}} < 0.75$ (Ledden & O'Dell 1985; Giommi et al. 1990; Stocke et al. 1985, 1991; Schachter et al. 1993). Padovani & Giommi (1995) introduced a broad-band spectral index (α_{rx}), to differentiate the two: $\alpha_{\mathrm{rx}} \leq 0.75$ for HBLs and $\alpha_{\mathrm{rx}} > 0.75$ for LBLs. Difference in the peak frequency distributions of RBLs and XBLs is another marker (Giommi, Ansari & Micol 1995; Padovani & Giommi 1995, 1996; Urry & Padovani 1995; Lamer, Brunner

& Staubert 1996). Sambruna et al. (1996) applied a logarithmic parabolic fit to multi-band flux data to obtain the peak frequencies, ν_p, of the synchrotron emission in their sample and sought to distinguish quantitatively RBL-like and XBL-like objects by means of the locations of these peak frequencies. Making use of ν_p calculated by Sambruna et al. (1996), Qin, Xie & Zheng (1999) found that all RBL-like objects are distributed in the region of $\log \nu_p < 14.7$, while most of XBL-like objects are located in the region of $\log \nu_p > 14.7$, with a few of them in the region of $\log \nu_p < 14.7$. In consideration of RBL-like objects and XBL-like objects have different dominant proper radiation mechanisms of the X-ray emission, Dong et al. (2002) recalculated ν_p of the synchrotron emission with the radio, optical and X-ray fluxes (F_r, F_o, F_x) of each source in the sample of Sambruna et al. (1996). They found that all RBL-like objects have $\log \nu_p < 14.7$; while all XBL-like objects have $\log \nu_p > 14.7$. This result indicates that α_{rx} is equivalent to $\log \nu_p$ as a classifying criterion, and provides certain evidence to support the suggestion of Giommi, Ansari & Micol (1995) that RBL-like and XBL-like objects can also be distinguished by the difference in the peak frequency of the synchrotron emission between them. Mei, Zhang & Jiang (2002) made a statistical analysis of the luminosities, broad-band spectral indexes and peak frequencies of the RBLs and XBLs in Sambruna et al. (1996). They found that HBLs and LBLs can be equally well distinguished by the radio luminosity L_r, therefore, α_{rx}, ν_p and L_r are equivalent in the classification of HBLs and LBLs (Mei, Zhang & Jiang 2002).

However, in a flux-limited sample covering especially a wide range of redshift, the use of luminosities instead of fluxes always introduces a redshift bias to the data, because the luminosity is strongly correlated with the redshift (Mücke et al. 1997; Fossati et al. 1998; Cheng, Zhang & Zhang 2002). It can be easily seen from Tables 1 and 2 that the redshifts of XBLs are almost of the same order and cover a range of Δz=0.53; but the redshifts of RBLs are not all of the same order and cover a much wider range of $\Delta z = 1.015$ (about twice the redshift range of XBLs). Therefore, it is very significant and necessary to estimate the influence of the luminosity–redshift relation on the dependence of the luminosity on other quantities. Since the flux density is less susceptible to such distortions (Cheng, Zhang & Zhang 2002), for simplicity we will directly make a comparison between the flux density distribution and the luminosity distribution in our sample. At the same time we will study the relations of the redshift with the flux density (F_r, F_o, F_x), the peak frequency ν_p and the broad-band spectral index α_{rx}, respectively; moreover we will reanalyze the relations of ν_p with the luminosity (L_r, L_o, L_x) and α_{rx} individually. The relevant data will be presented in Section 2. Our statistical analysis results will be given in Section 3 and then a discussion and conclusions will be presented in Section 4.

2 LUMINOSITY, BROAD-BAND INDEX AND PEAK FREQUENCY

Our sample consists of 70 BL Lacertae objects, including 33 RBLs and 37 XBLs. All of the RBLs and 30 of the XBLs originate from the complete 1 Jy sample of BL Lac objects and the Extended EMSS sample of BL Lac objects (for the latter, $F_x \geq 2 \times 10^{-13} \mathrm{erg\,cm^{-2}s^{-1}}$) presented respectively by Wolter et al. (1994), the other seven XBLs were selected from Stocke et al. (1991) and Sambruna et al. (1996). The reason behind this selection is to improve on the statistics. The relevant data for our sample, selected from the literature (Fossati et al. 1998; Sambruna et al. 1996; Wolter et al. 1994; Stocke et al. 1991), are listed in Tables 1 and 2. Column (1) gives the IAU name; Column (2), the redshift z; Column (3), the X-ray spectral index; Column (4), the broad-band spectral index; Column (5), the 5 GHz radio flux density (F_r) in Janskys; Column (6), the V band optical flux density (F_o) in millijanskys; Column (7), the 1 keV X-ray flux density (F_x) in microjanskys; Column (8), the peak frequencies; Column (9), the references for the foregoing parameters except where marked by a, b and c. For seven RBLs, we used lower limits for their redshifts, and five XBLs sources without redshift estimates, we assigned the average redshift of the EMSS sample, $\langle z \rangle = 0.30$. The X-ray power spectral indices for 14 sources in the EMSS sample and one source in the 1 Jy sample are not available, and a relevant mean value of $\langle \alpha_x \rangle = 1.30$ was assigned to the former and another value of $\langle \alpha_x \rangle = 1.01$ to the latter.

We first reduce the observed flux density at each energy band to the rest-frame by K-correction according to the formula $F = F_\nu^{ob}(1 + z)^{\alpha-1}$, where α is the spectral index ($F \propto \nu^{-\alpha}$), for RBLs $\alpha_r = 0.2, \alpha_o = 1.05$; and for XBLs $\alpha_r = 0, \alpha_o = 0.65$ (Falomo, Scarpa & Bersanelli 1994). For those objects with their individual X-ray spectral indices available we used these indices, but for those with no X-ray spectral indices we use the relevant mean value of the corresponding subclass, that is, $\langle \alpha_x \rangle = 1.30$ for

Table 1 The Einstein Observatory EMSS Sample of BL Lacertae Objects (XBLs)

Name	z	α_x	α_{rx}	F_r (Jy) (5 GHz)	F_o (mJy) (5500 Å)	F_x (μJy) (1 keV)	$\log \nu_p$ (Jm^{-2} s^{-1})	Ref
0112.1+0903	0.339	0.61	0.58	0.0014	0.047 ± 0.001	0.05	15.62[a]	(1)
0158.5+0019	0.299	1.46	0.51	0.0113	0.21 ± 0.06	1.2	17.34[a]	(1)
0205.7+3509	0.318	1.7	0.46	0.0036	0.10 ± 0.005	0.90	18.06[a]	(1)
0257.9+3429	0.247	1.67	0.65	0.01	0.25 ± 0.02	0.1	15.03[a]	(1)
0317.0+1834	0.19	1.32	0.58	0.017	0.36 ± 0.09	0.54	15.79[a]	(1)
0331.3−3629	0.308	...	0.64[b]	0.0087	0.15	0.07	15.079[b]	(2)
0350.0−3712	0.165	...	0.61[b]	0.0168	0.37	0.29	15.349[b]	(2)
0419.3+1943	0.512	0.72	0.53	0.008	0.09	0.75	18.31 [a]	(1)
0607.9+7108	0.267	1.21	0.7	0.0182	0.09	0.07	15.23[a]	(1)
0737.9+7441	0.315	0.91	0.56	0.024	0.64	1.3	16.09[a]	(1)
0922.9+7459	0.638	0.78	0.55	0.0033	0.044 ± 0.002	0.21	17.21[a]	(1)
0950.9+4929	0.207	1.76	0.51	0.0033	0.122 ± 0.04	0.27	16.13 [a]	(1)
0958.9+2102	0.344	...	0.59[b]	0.0015	0.04	0.03	15.389[b]	(3)
1019.0+5139	0.141	0.52	0.45	0.0024	0.22	0.93	16.69 [a]	(1)
1133.7+1618	...	...	0.65[b]	0.009	0.04	0.06	15.745[b]	(3)
1207.9+3945	0.615	1.13	0.52	0.0058	0.1	0.55	17.38 [a]	(1)
1221.8+2452	0.218	1.47	0.67	0.0264	0.42 ± 0.09	0.18	15[a]	(1)
1229.2+6430	0.164	0.99	0.56	0.042	0.55 ± 0.17	2.05	16.71[a]	(1)
1235.4+6315	0.297	1.91	0.55	0.007	0.14 ± 0.02	0.31	16.16[a]	(1)
1256.3+0151	...	...	0.67[b]	0.008	0.03	0.04	15.626[b]	(3)
1258.4+6401	...	...	0.66[b]	0.012	0.03	0.07	16.218[b]	(3)
1312.1−4221	0.108	...	0.51[b]	0.0185	0.51	2.11	16.756[b]	(2)
1332.6−2935	0.25	...	0.56[b]	0.0117	0.06	0.45	18.185[b]	(2)
1402.3+0416	0.2	1.85	0.57	0.0208	0.88 ± 0.37	0.68	15.39[a]	(1)
1407.9+5954	0.495	1.74	0.66	0.0165	0.07 ± 0.01	0.1	15.76[a]	(1)
1443.5+6349	0.299	1.1	0.58	0.0116	0.06	0.35	17.71[a]	(1)
1458.8+2249	0.235	2.31	0.58	0.0298	1.01 ± 0.20	0.78	15.39[a]	(1)
1534.2+0148	0.312	...	0.64[b]	0.034	0.09	0.30	16.714[b]	(2)
1534.8+0148	0.312	0.89	0.61	0.034	0.15 ± 0.05	0.74	17.4[a]	(1)
1552.1+2020	0.222	0.79	0.54	0.0375	0.44 ± 0.08	2.57	17.45[a]	(1)
1704.9+6046	0.28	...	0.55[b]	0.0018	0.08	0.08	15.574[b]	(3)
1757.7+7034	0.407	1.12	0.5	0.0072	0.18	0.92	17.15[a]	(1)
2143.3+0704	0.237	1.91	0.61	0.050	0.32 ± 0.04	0.78	16.24[a]	(1)
2306.1−2236	0.137	...	0.54[b]	0.0044	0.24	0.26	15.586[b]	(2)
2336.5+0517	...	...	0.6[b]	0.0049	0.03	0.08	16.372[b]	(3)
2342.7−1531	...	...	0.56[b]	0.0023	0.08	0.08	15.566[b]	(3)
2347.4+1924	0.515	...	0.57[b]	0.0032	0.02	0.08	17.011[b]	(3)

Notes: (1) Sambruna et al. (1996); (2) Stocke et al. (1991); (3) Wolter et al. (1994);[a] Dong et al. (2002); [b] Calculated by us.

14 XBLs and $\langle \alpha_x \rangle = 1.01$ for one RBL. Then we calculated the luminosity using $H_0 =70$ km s^{-1} Mpc^{-1} and $q_0 = 0.5$, assuming isotropic emission. Finally, for our 14 XBLs and four RBLs additional to the sample used by Dong et al. (2002), after taking the proper X-ray radiation mechanism of the two kinds of BL Lacertae objects into account, we calculated the peak frequencies ν_p after applying logarithmic parabolic fit to the data of flux densities, following Landau et al. (1996) and the broad-band index α_{rx} according to the definition (Ledden & O'Dell 1985; Sambruna et al. 1996).

3 ANALYSIS AND RESULTS

For an exploration of the effects of redshift on the luminosity, we plot the sources of our sample first in the flux-density/redshift plane, then in the luminosity/peak frequency plane. Then we will re-examine the relation of the peak frequency with the luminosity and the broad-band spectral index.

In Figure 1a, we plot F_r versus z for our sample. It can be easily seen: (1) The z distribution range of RBLs (squares and triangles) is about two times that of XBLs (circles). Note especially the five RBLs (comprising two HBLs denoted by triangles) have redshifts one order of magnitude smaller than the other RBLs and have larger F_r values than many of the others (see Fig. 1a, Table 2). (2) The F_r distribution range of RBLs is only half of that of XBLs. (3) A very large gap ($\triangle \log F_r = 1.03$) exists between the RBLs

Table 2 The Complete 1 Jy Sample of BL Lacertae Objects (RBLs)

Name	z	α_x	α_{rx}	F_r(Jy) (5 GHz)	F_o(mJy) (5500 Å)	$F_x(\mu$Jy) (1 keV)	$\log \nu_p$ (Jm^{-2} s^{-1})	Ref
0048−097	>0.2[a]	1.57	0.75	1.110 ± 0.583	2.41 ± 1.63	0.77	13.75	(1)
0118−272	>0.557	1.2	0.86	1.145 ± 0.075	1.92 ± 0.38	0.20	14.49	(1)
0235+164	0.94	1.79	0.76	1.81 ± 0.54	1.44 ± 1.06	1.56	13.39	(1)
0426−380	>1.03	0.95	0.9	1.15 ± 0.03	0.11	0.09	13.22	(1)
0454+844	0.112	1.43	1.01	1.41 ± 0.14	0.70 ± 0.36	0.02	13.81	(1)
0537−441	0.896	1.04	0.82	3.93 ± 0.42	1.49 ± 0.43	0.78	14.07	(1)
0716+714	>0.3	1.77	0.75	0.86 ± 0.18	2.96	1.17	13.79	(1)
0735+178	>0.424	1.2	0.88	2.13 ± 0.50	3.22 ± 1.56	0.22	14.03	(1)
0814+425	0.258	0.16	0.98	1.86 ± 0.68	0.26 ± 0.04	0.05	13.34	(1)
0820+225	0.951	1.05	0.996[b]	0.846	0.07	0.052	13.08[b]	(2)
0823+033	0.506	...	0.87[b]	0.976	0.869	0.30[a]	13.39[b]	(2)
0828+493	0.548	0.68	0.99[b]	0.665	0.138	0.035	13.01[b]	(2)
0851+202	0.306	1.38	0.84	2.99 ± 0.56	6.08 ± 5.91	0.70 ± 0.25	13.72	(1)
0954+658	0.367	0.24	0.88	0.90 ± 0.38	0.86 ± 0.24	0.16	14.09	(1)
1144−379	1.048	1.54	0.82	1.61 ± 0.96	0.62 ± 0.37	0.41	13.75	(1)
1147+245	>0.2[a]	0.86	0.92	0.82 ± 0.12	1.53 ± 0.36	0.05	14.58	(1)
1308+326	0.997	0.95	0.91	2.26 ± 0.40	2.23 ± 1.53	0.13	13.83	(1)
1418+546	0.152	1.12	0.85	1.22 ± 0.38	2.72 ± 0.82	0.3	13.85	(1)
1514−241	0.049	0.61[c]	0.85[b]	1.907	5.474	0.607	14.56[b]	(2)
1519−273	>0.2[a]	1.03	0.86	2.17 ± 0.25	0.47 ± 0.35	0.39	13.17	(1)
1538+149	0.605	0.66	0.93	1.53 ± 0.42	0.32 ± 0.10	0.09	13.56	(1)
1652+398	0.033	1.63	0.67	1.27 ± 0.10	15.65 ± 4.52	8.3	15.01	(1)
1749+096	0.32	0.63	0.92	1.44 ± 0.36	1.18 ± 0.54	0.14 ± 0.01	13.27	(1)
1749+701	0.77	1.77	0.81	1.11 ± 0.35	0.99 ± 0.22	0.15	14.43	(1)
1803+784	0.679	1	0.88	2.79 ± 0.30	0.99 ± 0.22	0.26 ± 0.03	13.43	(1)
1807+698	0.051	0.81	0.87	1.71 ± 0.32	7.85 ± 2.44	0.32	14.26	(1)
1823+568	0.664	0.15	0.85	1.45 ± 0.21	0.17	0.42	13.65	(1)
2005−489	0.071	1.99	0.71	1.21 ± 0.02	9.85 ± 1.71	4.12 ± 1.77	14.86	(1)
2007+777	0.342	0.66	0.91	1.72 ± 0.41	1.17 ± 0.18	0.17	13.66	(1)
2131−021	0.557?	1.05	0.96	1.84 ± 0.31	0.16 ± 0.04	0.05	13.16	(1)
2200+420	0.069	0.95	0.85	3.51 ± 1.96	8.65 ± 4.62	0.88	14.25	(1)
2240−260	0.774	1.15	0.89	1.03	0.26 ± 0.10	0.07	13.32	(1)
2254+074	0.19	1.12	0.88	0.56 ± 0.27	0.6 ± 0.19	0.09	13.25	(1)

Notes: (1) Sambruna et al. (1996); (2) Fossati et al. (1998); [a] Wolter et al. (1994); [b] Calculated by us; [c] Xie et al. (2001).

and the XBLs. For example, the lines $\log F_r = -0.33$ and -1.39 can be regarded as thresholds for the two populations. There is no such clear separation between the LBLs and HBLs. In addition, there is no correlation between $\log F_r$ and $\log z$ (the formal correlation coefficient is $r = 0.013$).

However, Figure 1b exhibits: (1) The L_r distribution range of RBLs is now about 1.5 times that of XBLs. (2) Although the gap between the two populations is now smaller ($\triangle \log L_r = 0.26$), it can separate not only the RBLs and XBLs (for example, by the line $\log L_r = 42.65$) but also the LBLs and HBLs by such lines as $L_r = 43.30$. The reason behind this difference is obviously due to the influence of redshift on the radio luminosity, which makes the distribution of radio luminosity different from that of radio flux density in our sample. One can see that the five RBLs, denoted by triangles, have larger F_r values than many of RBLs but nearly the smallest L_r values among the RBLs because of their very small redshifts (see Fig. 1, Table 2). That is, although the five RBLs are located in the range of relatively larger F_r values, they are almost systematically below the other RBLs in the distribution of L_r. Especially the two HBLs (1652+398 and 2005−489, denoted by the two filled triangles) are located below the other RBLs (see Fig. 1, Table 2). A simple linear regression analysis gives a strong negative correlation between $\log L_r$ and $\log \nu_p$, namely

$$\log L_r = -(0.68 \pm 0.06) \log \nu_p + (53.30 \pm 0.95), \tag{1}$$

with chance probability $p = 6.09 \times 10^{-16}$ and correlation coefficient $r = -0.799$ (see Fig. 1b).

Figure 2a plots $\log F_o$ versus $\log z$; it shows that there is no correlation between the two (the formal correlation coefficient is $r = -0.399$). From Figure 2a and 2b we can see that the distribution of L_o is also obviously different from that of F_o for the sample. About 3/4 of the XBLs and more than 1/2 of the
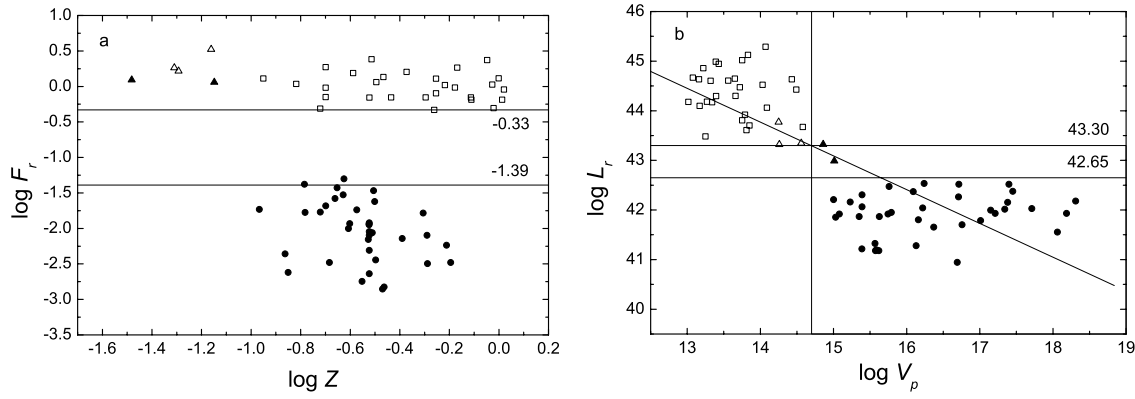
Fig. 1 Comparison between the distributions of radio flux density and radio luminosity: (a) $\log F_r$ versus $\log z$; (b) $\log L_r$ versus $\log \nu_p$. The filled circles represent the XBLs; the open squares a majority of RBLs, and the triangles the five RBLs with redshifts one order of magnitude lower than the majority's. All filled symbols stand for HBLs and all open symbols for LBLs.
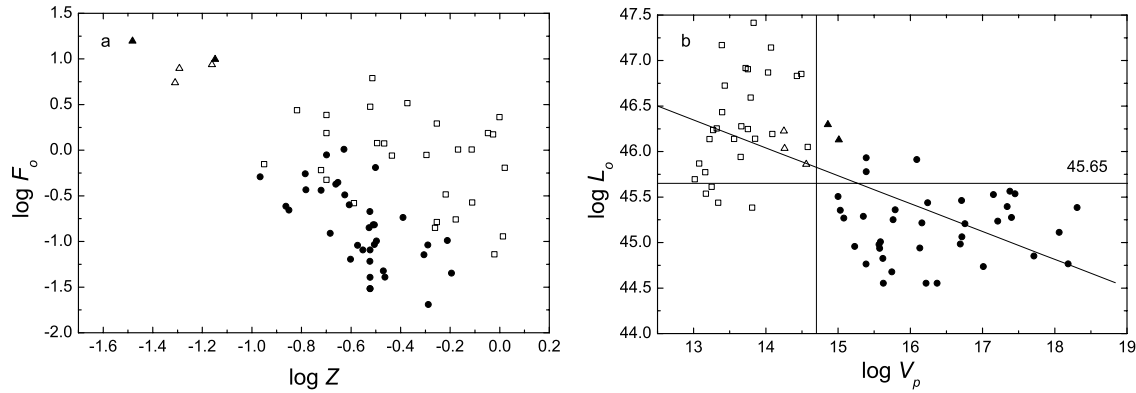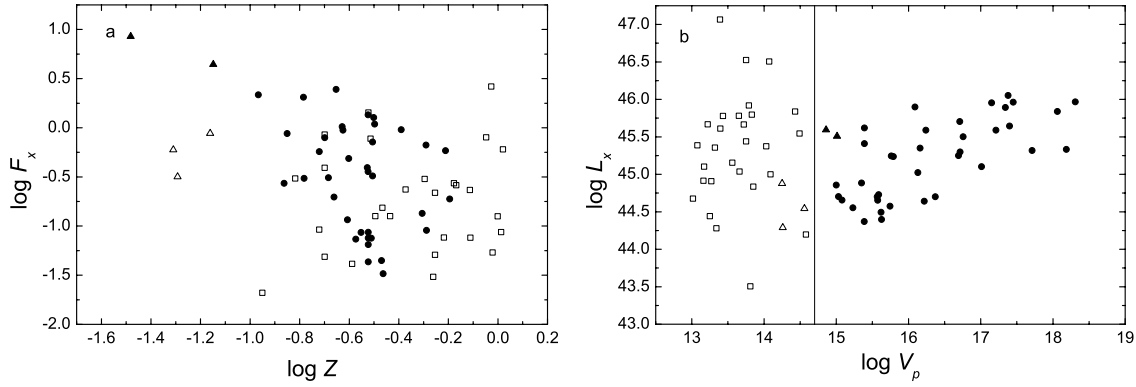

Fig. 2 Comparison between the distributions of optical flux density and optical luminosity: (a) $\log F_o$ versus $\log z$; (b) $\log L_o$ versus $\log \nu_p$. The filled circles stand for the XBLs; the open squares a majority of the RBLs, and the triangles the five of RBLs whose redshifts are one order of magnitude lower than the majority's. All filled symbols represent HBLs and all open symbols for LBLs.

RBLs overlap in the same $\log F_o$ distribution range (see Fig. 2a), but almost all the RBLs are in the range of $\log L_o > 45.65 (\mathrm{mJy\,s^{-1}})$ except for four sources, while all but three XBLs are in the range $\log L_o < 45.65 (\mathrm{mJy\,s^{-1}})$ (see Fig. 2b). This fact implies that the RBLs and XBLs of the sample cover almost different ranges of L_o but occupy the same range of F_o. The horizontal line of $\log L_o = 45.65 (\mathrm{erg\,s^{-1}})$ can almost give a clear separation between RBLs (above) and XBLs (below) (see Fig. 2b). Between $\log L_o$ and $\log \nu_p$, a very significant negative correlation is found:

$$\log L_o = -(0.31 \pm 0.04) \log \nu_p + (50.33 \pm 0.67), \tag{2}$$

with chance probability $p = 5.22 \times 10^{-9}$ and correlation coefficient $r = -0.643$ (see Fig. 2b).

Figure 3a shows that there is also no correlation between $\log F_x$ and $\log z$ (formal correlation coefficient $r = -0.333$). A simple comparison between Figure 3a and 3b shows that there are also significant differences between the distributions of $\log F_x$ and $\log L_x$: the $\log F_x$ distribution range of RBLs is 1.40 times of that of XBLs (see Fig. 3a), but the $\log L_x$ distribution range of RBLs becomes about 2.12 times of that of XBLs (see Fig. 3b). Similarly, the five RBLs are mostly located in the mid-lower L_x distribution

Fig. 3 Comparison of the distributions between the X-ray flux density and the X-ray luminosity: (a) $\log F_x$ versus $\log z$; (b) $\log L_x$ versus $\log \nu_p$. The filled circles represent XBLs; the open squares a majority of RBLs, and the triangles for the five RBLs whose redshifts are one order of magnitude lower than the majority's. All filled symbols stand for HBLs and all open symbols for LBLs.

region of RBLs but in the mid-upper F_x distribution region of RBLs (see Fig. 3a and 3b). However, in this case no correlation is found between $\log L_x$ and $\log \nu_p$ (correlation coefficient only $r = 0.144$) (see Fig. 3b), it is a little different from that addressed above.

Figure 4a and 4b respectively plot the peak frequency and the broad-band spectral index against the redshift (respective correlation coefficients $r = -0.157$ and $r = 0.193$). They show that there is no correlation of the redshift with the peak frequency or the broad-band spectral index with the redshift. However, Figure 4c shows that there is a strong negative correlation between the peak frequency and the broad-band spectral index, namely,

$$\log \alpha_{rx} = -(0.09 \pm 0.01) \log \nu_p + (2.16 \pm 0.09) \tag{3}$$

with its chance probability $p = 1.87 \times 10^{-23}$ and correlation coefficient $r = -0.887$ (see Fig. 4c). More importantly, one can see that the lines $\alpha_{rx} = 0.75$ and $\log \nu_p = 14.7$ divide the plane neatly into four quadrants, with all HBLs falling in the fourth and all LBLs in the second.

4 DISCUSSION AND CONCLUSIONS

A statistical analysis of our compiled sample shows that the flux densities (F_r, F_o, F_x) are not correlated with the redshift, but the luminosity/redshift relation indeed induces an effect on the luminosity distribution, which shows up in an obvious difference between the flux density and luminosity distributions. That is, the redshift effect makes HBLs and LBLs cover the two separated distribution ranges of the radio luminosity; for optical band it greatly decreases the superposed distribution probability of RBLs and XBLs and almost makes both of them occupy two different optical luminosity distribution ranges; and for X-ray band it significantly increases the overlapping probability in X-ray luminosity distribution of RBLs and XBLs.

Secondly, our linear regression analysis shows different relations between the peak frequency and each of the different band luminosities: (1) There is a strong negative correlation between $\log L_r$ and $\log \nu_p$ and a very significant negative correlation between $\log L_o$ and $\log \nu_p$. (2) No correlation is found between $\log L_x$ and $\log \nu_p$. These results support the suggestion that the location of the peak frequency, ν_p, is linked to the luminosity (Sambruna et al. 1996), but not always linked to the luminosity in any wave band because the relations between them are different for different wave bands.

Finally, our analysis indicates that the broad-band spectral index and the peak frequency have no correlations with the redshift, but they are negatively correlated strongly to each other. That is, the higher the peak frequency, the flatter the broad-band spectral index. More importantly, $\alpha_{rx} = 0.75$, like $\log \nu_p = 14.7$, can be used to be a boundary between HBLs and LBLs. It offers a support for the assumption that the synchrotron peak frequency can be derived from the values of the broad-band spectral index (Urry & Padovani 1995; Maraschi et al. 1995; Comastri et al. 1995; Comastri et al. 1997; Caccianiga et al. 2004; Fossati et al. 1998).
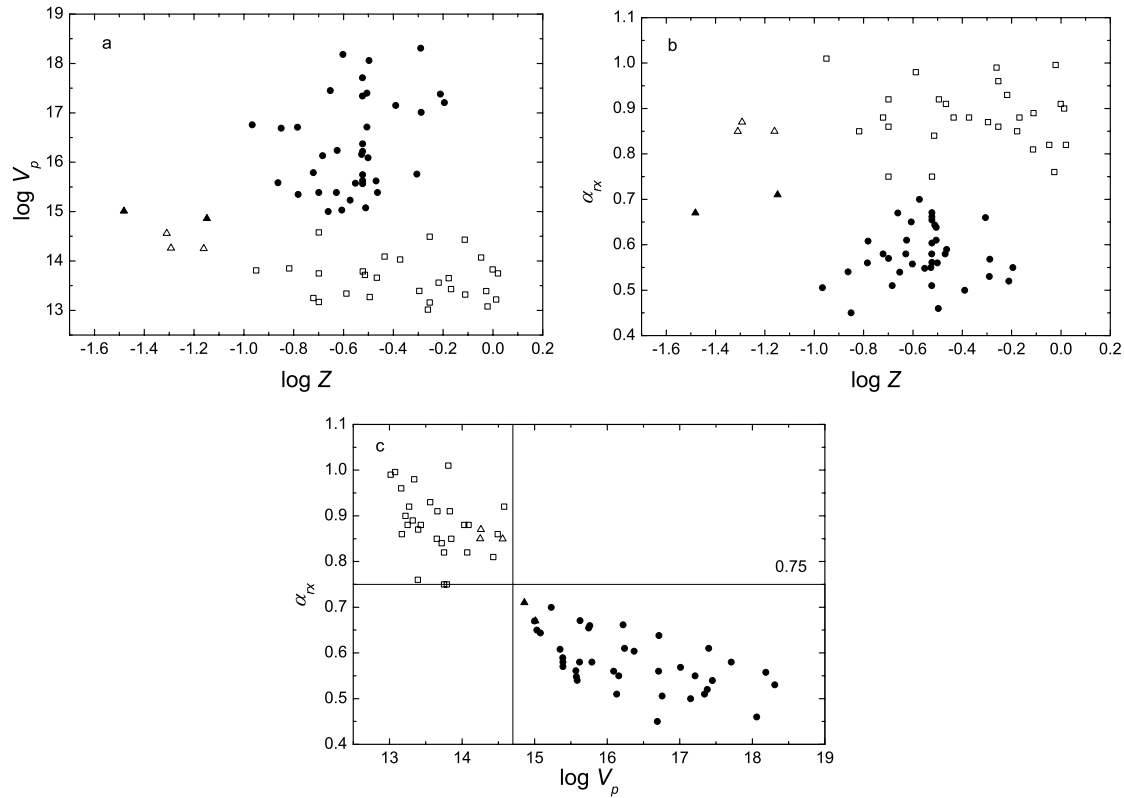
Fig. 4 No effect of redshift on the peak frequency and the broad index: (a) $\log \nu_p$ versus $\log z$; (b) α_{rx} versus $\log z$; (c) α_{rx} versus $\log \nu_p$. The filled circles stand for XBLs, the open squares for a majority of the RBLs, and the triangles the five of RBLs whose redshifts are one order of magnitude lower than the majority's. All filled symbols stand for HBLs and all open symbols for LBLs.

Why is there the strong correlation between α_{rx} and $\log \nu_p$? and why are there the different relations between the peak frequency and the luminosity at different wave bands? The reasons behind these observed facts may mainly originate from the following. First, the peak energy of the equilibrium particle distribution in the jet is determined by a balance between the processes of radiative cooling and particle acceleration. If the radiative cooling process is weaker, the equilibrium particle distribution will peak at a higher energy; and conversely. Therefore, the less powerful objects will peak at higher energy bands, the more powerful objects, at lower energy bands (Ghisellini et el. 1998). Secondly, the high-energy emission continuum in blazars is characterized by their X-ray spectral indices, this point has been confirmed by BeppoSAX observations of BL Lac objects (Wolter et al. 1998; Padovani et al. 2001). Finally, Fossati et al. (1998) found that there is a good anti-correlation between α_x and L_r, which shows that the blazar sequence follows a transition from the synchrotron to the inverse Compton in the X-ray regime with the radio luminosity increasing (peak frequency decreasing).

Therefore, our conclusions are the following. Because there are no redshift effects on the broad band index and peak frequency, these two classifying criteria of BL Lac objects are equivalent and both can still be used to distinguish HBLs from LBLs for our enlarged sample. However, there are significant influences of the luminosity-redshift relation on the luminosity distribution in the observed sample, the effects of which are different in different wave bands. Obviously it is just these influences that enable the radio luminosity to distinguish between HBLs and LBLs. From this point of view, the radio luminosity, to be used as a classifying criterion of BL Lac objects, should not be regarded as equivalent to the broad-band index or the peak frequency. It may be probably regarded as a result of evolutionary effects genuinely related to redshift (Fossati et al. 1998; Xie et al. 2001b).

We have also supplied a specific piece of evidence for the suggestion that in a flux-limited sample covering especially a wide range of redshifts, the use of luminosities instead of fluxes always introduces a redshift bias to the data, because the luminosity is strongly correlated with redshift (Mücke et al. 1997; Fossati et al. 1998; Cheng, Zhang & Zhang 2002).

References

Caccianiga A., Marchã M. J. M., 2004, MNRAS, 348, 937
Cheng K. S., Zhang X., Zhang L., 2002, ApJ, 533, 80
Comastri A., Molendi S., Ghisellini G., 1995, MNRAS, 277, 297
Comastri A., Fossati G., Ghisellini G. et al., 1997, ApJ, 480, 534
Dong Y.M., Mei D.C., Liang E.W., 2002, PASJ, 54, 171
Falomo R., Scarpa R., Bersanelli M., 1994, ApJS, 93, 125
Fossati G., Maraschi L., Celotti A. et al., 1998, MNRAS, 299, 433
Ghisellini G., Maraschi L., Treves A. et al., 1986, ApJ, 310, 317
Ghisellini G., Celotti A., Fossati G. et al., 1998, MNRAS, 301, 451
Giommi P., Barr P., Pollock A. M. T. et al., 1990, ApJ, 356, 432
Giommi P., Padovani P., 1994, MNRAS, 268, L51
Giommi P., Ansari S. G., Micol A., 1995, A&AS, 109, 267
Lamer G., Brunner H., Staubert R., 1996, A&A, 311, 384
Landau R., Golisch B., Jones T. J. et al., 1986, ApJ, 308, 78
Ledden J. E., O'Dell S. L., 1985, ApJ, 298, 630
Maraschi L., Ghisellini G., Celotti A., 1992, ApJ, 397, L5
Maraschi L., Fossati G., Tagliaferri G., Treves A., 1995, ApJ, 443, 578
Mei D. C., Zhang L., Jiang Z. J., 2002, A&A, 391, 917
Mücke A., Pohl M., Reich P. et al., 1997, A&A, 320, 33
Padovani P., Giommi P., 1995, ApJ, 444, 567
Padovani P., Giommi P., 1996, MNRAS, 279, 526
Padovani P. et al., 2001, MNRAS, 328, 931
Qin Y. P., Xie G. Z., 1997, ApJ, 487, L41
Qin Y. P., Xie G. Z., Zheng X. T., 1999, Ap&SS, 266, 549
Sambruna R. M., Maraschi L., Urry C.M., 1996, ApJ, 463, 444
Schachter J. F., Stocke J. T., Perlman E. et al., 1993, ApJ, 412, 541
Stocke J. T., Liebert J., Schmidt G. et al., 1985, ApJ, 298, 619
Stocke J. T., Morris S. L., Gioia I. M. et al., 1991, ApJS, 76, 813
Urry C. M., Padovani P., 1995, PASP, 107, 803
Wolter A., Caccianiga A., Roberto D. C. et al., 1994, ApJ, 433, 29
Wolter A. et al., 1998, A&A, 335, 899
Xie G. Z., Dai B. Z., Liang E. W. et al., 2001a, PASJ, 51, 469
Xie G. Z., Dai B. Z., Mei D. C. et al., 2001b, Chin. J. Astron. Astrophys. (ChJAA), 1, 213
Xie G. Z., Ding S. X., Dai H. et al., 2003, Int. J. Mod. Phys. D, 12, 781